NASA TECHNICAL MEMORANDUM

NASA TM X-62,189

NASA TM X-62,189

PRESSURE–FLUCTUATION INPUTS AND RESPONSE OF PANELS UNDERLYING ATTACHED AND SEPARATED SUPERSONIC TURBULENT BOUNDARY LAYERS

Charles F. Coe and Wei J. Chyu

Ames Research Center
Moffett Field, Calif. 94035

Technical paper presented at AGARD Symposium on Acoustic Fatigue
Toulouse, France, September 26–27, 1972

September 1972

PRESSURE-FLUCTUATION INPUTS AND RESPONSE OF PANELS UNDERLYING ATTACHED AND SEPARATED SUPERSONIC TURBULENT BOUNDARY LAYERS

by

Charles F. Coe
Chief, Aeronautical Structures Branch
and
Wei J. Chyu, Scientist
Ames Research Center, NASA, Moffett Field, California 94035, USA

SUMMARY

The paper summarizes results of an investigation of surface pressure fluctuations and response of panels underlying attached and separated turbulent boundary layers and shock waves at NASA Ames Research Center. Extensive tests of a large assortment of axisymmetric and two-dimensional models have been conducted at transonic and supersonic Mach numbers to 3.6 to study the pressure fields. Assorted fixed-edge flat panels have been tested at Mach numbers from 1.6 to 3.6 in attached and completely separated flow fields and also in mixed flow with a step induced shock wave oscillating on the panels. The surface pressure fluctuations are described in terms of broad-band rms, spectral density, and spatial correlation information. The effectiveness of parameters for scaling the pressure fluctuations is also illustrated. Measurements of the amplitude and strain response of the panels are compared with response computations by the normal mode method of analysis.

NOTATION (Note: All dimensions in standard metric units)

A	surface area of the panel
A_m	normalization factor for ψ_m
$B = \frac{Eh^3}{12(1-\nu^2)}$	bending stiffness
c	damping coefficient
C_p	static pressure coefficient, $(p-p_\infty)/q_\infty$
d	thickness of panel
D	diameter
E	Young's modulus
f	frequency
$f_\alpha(t)$	generalized force
$f\ell/U_c$	Strouhal number
$F_1 = 4f\ell_1/U_c$	
$F_2 = 4f\ell_2/U_c$	
F_α	Fourier transform of f_α
$G(\omega) = 2S(\omega)$	one-sided power spectral density function
$G(\xi, \omega) = 2S(\xi, \omega)$	one-sided cross spectral density
h	shoulder height of cone frustum or two-dimensional wedge
$H_\alpha(\omega)$	frequency response function
$j_{mr}(\omega)$	real part of longitudinal acceptance
$j'_{ns}(\omega)$	transversal acceptance
$k_{mr}(\omega)$	negative of imaginary part of longitudinal acceptance
ℓ_1	panel length in x_1 direction
ℓ_2	panel length in x_2 direction
m_α	generalized mass for the αth mode
M_∞	free stream Mach number
p	local static pressure
$\tilde{p}(x,t)$	pressure fluctuation acting on the panel
q_∞	free stream dynamic pressure
$q_\alpha(t)$	generalized coordinates
$Q_\alpha(\omega)$	Fourier transform of q_α
$S(\underline{x}', \underline{x}'', \omega)$	two-sided cross spectral density function
$S(\underline{x}, \omega)$	two-sided power spectral density function
S_s	flow separation length measured upstream from $x_s = 0$
t	time
U	velocity
$U_c(f)$	narrow-band convection velocity
$w(\underline{x}, t)$	displacement normal to the panel surface
$W(\underline{x}, \omega)$	Fourier transform of w
x_s	longitudinal distance measured upstream from shoulder of cone frustum or two-dimensional wedge
x_1	location on the panel in the longitudinal (or streamwise) direction
x_2	location on the panel in the lateral direction

$\underline{x}(x_1, x_2)$	coordinate referring to location on the panel
$y_1 = x_1/\ell_1$	
$y_2 = x_2/\ell_2$	
$\underline{y}/y_1, y_2)$	normalized coordinates referring to location on the panel
δ	boundary layer thickness
$\delta*$	displacement boundary layer thickness
$\delta_{\alpha\beta}$	Kronecker delta
$\nabla^4 = \frac{\partial^4}{\partial x_1^4} + 2\frac{\partial^2}{\partial x_1^2}\frac{\partial^2}{\partial x_2^2} + \frac{\partial^4}{\partial x_2^4}$	
$\underline{\xi} = \underline{x}' - \underline{x}''$	coordinate referring to the separation distance of two points on the panel
$\eta_1 = y_1' - y_1''$	
$\eta_2 = y_2' - y_2''$	
$\underline{\eta}(\eta_1, \eta_2) = \underline{y}' - \underline{y}''$	
ϵ	strain
μ	mass per unit area of the panel
ν	Poisson ratio
ν_α	loss factor for the αth mode
α	attenuation coefficient
γ	coherence function
θ	angle of cone frustum or wedge
ρ	correlation coefficient
$\psi_\alpha(\underline{x})$	mode shape function of the panel
$\bar{\psi}_\alpha(\underline{y})$	mode shape function of a panel with unit dimensions
ω	angular frequency
ω_α	natural frequency of the αth mode
ϕ	phase angle of cross spectral density function

Subscripts

norm	normalized quantity
$\alpha = (m, n)$	mode index
$\beta = (r, s)$	mode index
o	quantity evaluated immediately ahead of detached shock wave
∞	quantity evaluated at the free stream
1	streamwise direction
2	lateral direction
p	quantities related to the excitation field
d	quantities related to panel displacement
ϵ	quantities related to strain

1. INTRODUCTION

The pressure fluctuations in regions of attached and separated turbulent boundary layers and shock waves adjacent to surface of aerospace vehicles give rise to structural vibrations throughout atmospheric flight. The study of these excitations and resulting vibrations is of importance in determining stress, fatigue life of structures, and noise transmission into the interior of the vehicle. Unfortunately, the analysis of this type of vibration is complicated by the inherent random characteristics of the excitation pressure fields, and the difficulty of analytically describing the vibration of a realistic structure. For these reasons, early investigators of this problem considered only a hypothetical flow field and made the simplifying assumption that the structure, almost invariably either a beam or a rectangular panel, is infinitely large (refs. 1-3). This assumption gives rise to a solution in terms of the mean square displacement of the panel as a whole, but not the displacement as a function of location on the panel.

Investigations dealing with the excitation fields for the attached and separated turbulent boundary layers and regions of mixed flow, including oscillating shock waves, have been numerous (the references of refs. 4-6 yield an appropriate lengthy bibliography). A review of the literature indicates, however, that the required statistical information to describe the surface-pressure fluctuations is reasonably complete only for subsonic attached turbulent boundary layers. Investigations at transonic and supersonic speeds have primarily included measurements of pressure-fluctuation intensities and very limited analysis of power spectra and/or spatial correlation. With the exception of results in references 4-7, these latter forms of analyses have only been published for attached flow.

With respect to response, recent investigations have considered finite-size rectangular panels underlying subsonic attached turbulent boundary layers, but a simplifying assumption was made that the panels were simply supported (refs. 8-10). This assumption simplifies the algebra tremendously, permitting solutions to be expressed in closed forms; and although these analytical results give better agreement with experiment than those obtained with the infinite panel assumption, they tend to overestimate the response of a realistic panel. Previous analyses also failed to give an accurate prediction of the wave matching between the flexural wave of a panel and the pressure wave. The estimation of this wave matching is important particularly when the matching occurs at one of the resonant frequencies of the structure and this causes a large structural response. With the advent of modern high speed computers, a theoretical analysis of a finite rectangular panel with clamped edges under the excitation of a turbulent boundary

layer is now feasible. Analytical integration in closed forms are not necessary, since numerical integration can be carried out with no algebraic simplification of the integrand. This digital-computer-oriented approach has the following additional advantages over an analytical approach: (1) The transparency of the problem is preserved, as very often the physics of the problem is lost amongst a great length of closed-form mathematical formulae; (2) future developments are simplified as the basic computer program can be modified to describe different flow fields and/or different structures.

With the deficiencies in both the input and response problems in mind, a research program has been undertaken at NASA, Ames Research Center, to improve the statistical description of the random pressure fluctuations underlying attached and separated turbulent boundary layers and shock waves; and to improve the analytical capability for computation of the displacement and strain of realistic panel structures when excited by each of these flow fields. The investigations of pressure fluctuation inputs and response have spanned the subsonic, transonic, and supersonic speed ranges up to a Mach number of 3.5.

Sketches of models used for the investigation of pressure-fluctuation inputs are shown in Fig. 1. The basic configurations were 0.0508 m and 0.254 m diameter ogive cylinders and the Ames 9- by 7-foot and 8- by 7-foot supersonic wind tunnel (SWT) walls to investigate attached turbulent boundary-layers. Cone frustums ahead of axisymmetric rings and two-dimensional wedges of different heights and a variety of angles from 15° to 90° were added to the cylinders and walls to investigate regions of separated flow and shock waves. The different model sizes and tunnel walls provided large variations of the thicknesses of both the attached and separated boundary layers to investigate scaling relationships to establish the most effective parameters for nondimensionalization of the pressure fluctuations. The thickness of attached boundary layers, for example, varied from approximately 0.00406 m on the 0.0508 m diameter model to 0.135 m on the wind-tunnel wall. Separated-flow lengths ahead of 45° frustums and a 0.2032 m high 45° wedge varied from 0.041 m to 0.89 m.

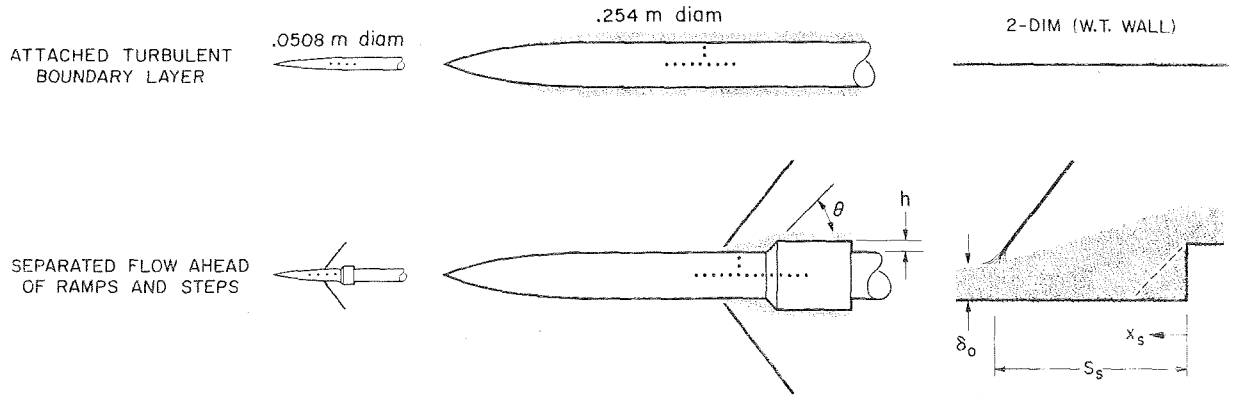

Figure 1. Configuration investigated for study of surface-pressure fluctuations.

The surface pressure fluctuations were measured with two different sizes of semiconductor type pressure transducers having sensing diameters of 0.00279 m and 0.00121 m. The transducers were mounted flush or slightly submerged to the surface in longitudinal, lateral, and diagonal arrays. In addition, detailed static-pressure distributions and boundary-layer measurements were obtained. More details on the test procedure, data acquisition and analysis, and overall scope of the pressure-fluctuation investigation can be found in references 4 and 7.

For the response part of the research, the first step in the program was to develop the analytical capability and a practical computer program for computation of the amplitude response of a clamped-edge panel. The excitation of a subsonic attached turbulent boundary layer was considered first because of the availability of corresponding excitation data by Bull (ref. 11), and response measurements by Wilby (ref. 10). The method of analysis (method of normal mode used together with the technique of spectral analysis) and comparisons with Wilby's response data are shown in reference 12. These initial results show favorable comparisons between the computed and measured response.

The analysis and computer program have subsequently been expanded to include the amplitude and strain response of simply-supported and clamped-edge panels excited by supersonic attached and separated turbulent boundary layers. Corresponding experiments have been conducted to measure the amplitude and strain response of a variety of panels with different length-to-width ratios and thicknesses. Panel lengths and widths varied from 0.1524 m to 0.3045 m and thicknesses varied from 0.5588×10^{-3} m to 2.234×10^{-3} m. The tests were conducted in the same facilities (9- by 7-foot SWT and 8- by 7-foot SWT) used for the supersonic pressure-fluctuation studies between Mach numbers of 1.6 and 3.5. An illustration of the test set up for separated flow is shown in Fig. 2. The panel response tests were conducted with the 0.2032-m high 90° step, whereas pressure fluctuations were also measured ahead of 23° and 45° wedges. Separated flow lengths ahead of the steps varied from approximately 0.91 m to 1.10 m depending on Mach number and the attached boundary layer thickness.

Three test conditions with the panels underlying attached flow, separated flow, and mixed flow with an oscillating shock wave were investigated. Attached flow was obtained by removing the step. Separated flow was obtained with the step positioned as shown in Fig. 2 so that the panel was about one-third the distance between the shock wave and the step. The step was moved further downstream to position the shock wave on the panels.

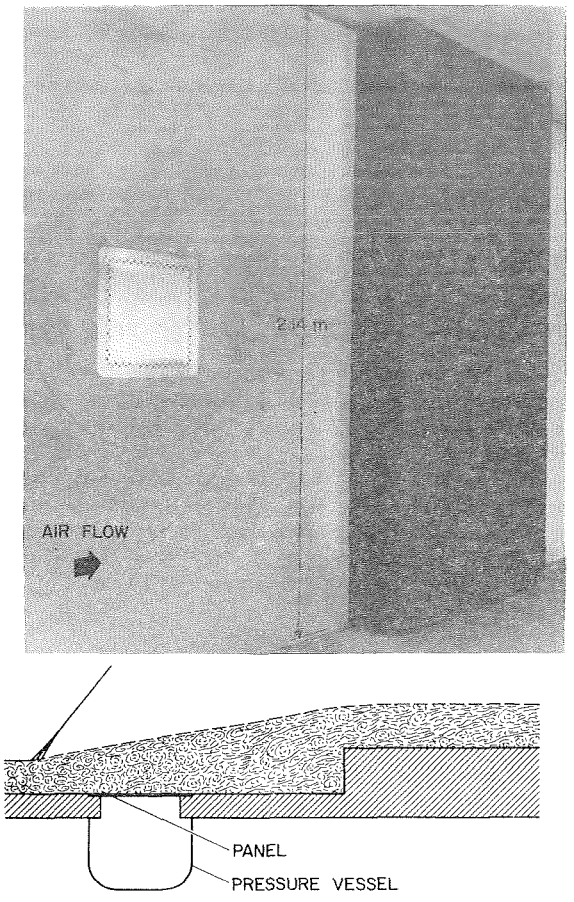

Figure 2. Panel-response test installation.

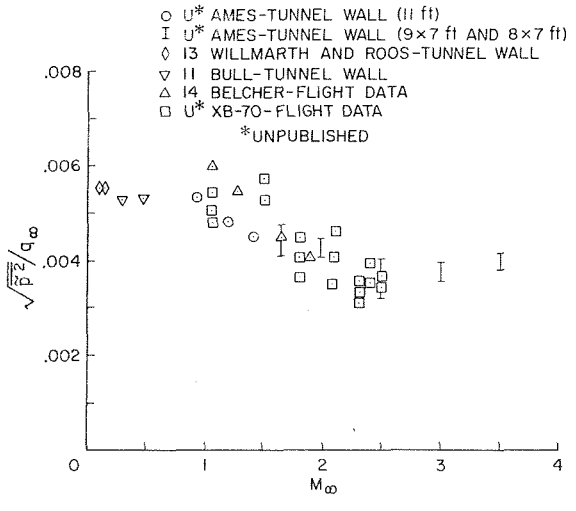

Figure 3. Broadband characteristics of pressure fluctuations underlying attached turbulent boundary layers.

Panel displacements were measured with non-contacting capacitance probes that could be remotely positioned to different panel coordinate positions. A steady-state cavity pressure was carefully maintained at wall static pressure at the streamwise midpoint near the lower edge of the panels for all test conditions.

The analyses of all the results of the pressure fluctuation and panel response investigations are not complete. However, a large amount of data have been amassed for attached and separated flows at supersonic speeds, and therefore these data and the corresponding panel response measurements and analyses are the subject of this paper.

2. PRESSURE-FLUCTUATION INPUTS

2.1 Broadband Characteristics

The surface-pressure fluctuations measured in attached flow on the walls of Ames wind tunnels are shown in Fig. 3 along with comparative data from a few other investigations. The data presented are considered by the authors to most reliably represent the broadband intensities of the pressure fluctuations, $\sqrt{\overline{p^2}}/q_\infty$, for the Mach number range from 0 to 3.5. Many more data points could be added to the figure from other earlier investigations, but the spread of data would then be increased markedly. Most of the other available data considered have been rejected because of uncertain effects of transducer size, installation, and extraneous noise. The data from the Ames 9- by 7-foot SWT and 8- by 7-foot SWT and the XB-70 represent measurements at several locations on a rigid plate in the tunnel wall and on the aircraft. The spread in data of about 30% (3 dB) is typical and is believed due to a nonuniformity in the unsteady pressure field. The fact that data can be consistently repeated within 0.3 dB when different transducers of the same kind are installed at a specific location on the wind tunnel wall supports this argument. Generally, the wind tunnel and flight data in Fig. 3 compare favorably, and both show about a 50% decrease in $\sqrt{\overline{p^2}}/q_\infty$ between Mach numbers of 1 and 2.5. At $M > 2.5$ the available wind tunnel data show a tendency for $\sqrt{\overline{p^2}}/q_\infty$ to increase slightly from a minimum of about 0.0035 at $M = 2.5$ to about 0.004 at $M = 3.5$.

Typical longitudinal distributions of mean static and fluctuating pressures illustrative of the separated flow on the models of this investigation are shown in Fig. 4 (the effect of diameter and frustum height in Fig. 4(a) and the effect of Mach number on the flow field in the vicinity of the response-test panel is shown in Fig. 4(b)). As previously described (refs. 4 and 15), the mean static pressure, initially at free-stream static pressure, increases rapidly as the flow encounters the detached frustum shock near the separation point and then approaches a plateau as the transition from attached to separated flow is completed. The static-pressure coefficients in the region of the plateau were nearly the same on all the axisymmetric models, but were approximately 20% lower than the corresponding measurements on the two-dimensional wall. The locations of the static-pressure rise associated with the shocks and separation points were not scaled by the x_s/h parameter. Further study of the shock separation distances has shown that the differences are due to the variation of h/δ_o on these models rather than to Reynolds number effects.

The characteristic feature of the broadband pressure fluctuations (Fig. 4(a)) can be related to features of the mean static-pressure distributions. The pressure fluctuations increase rapidly at the shock, as identified by the rapid pressure rise, and reach a maximum intensity where the slope of the static-pressure curve is maximum. In the fully separated region, the fluctuating pressure descends from this maximum to a plateau level. Correspondingly in this same region the static pressure descreases toward a plateau level. It can be noted that the plateau level was relatively independent of the shoulder height of the frustum that caused the separation on the 0.254-m-diameter models. The lower fluctuating-pressure intensities on the 0.0508-m-diameter model were found to be due to an insufficient frequency range of the recorded data. The higher fluctuating pressures on the two-dimensional model are associated

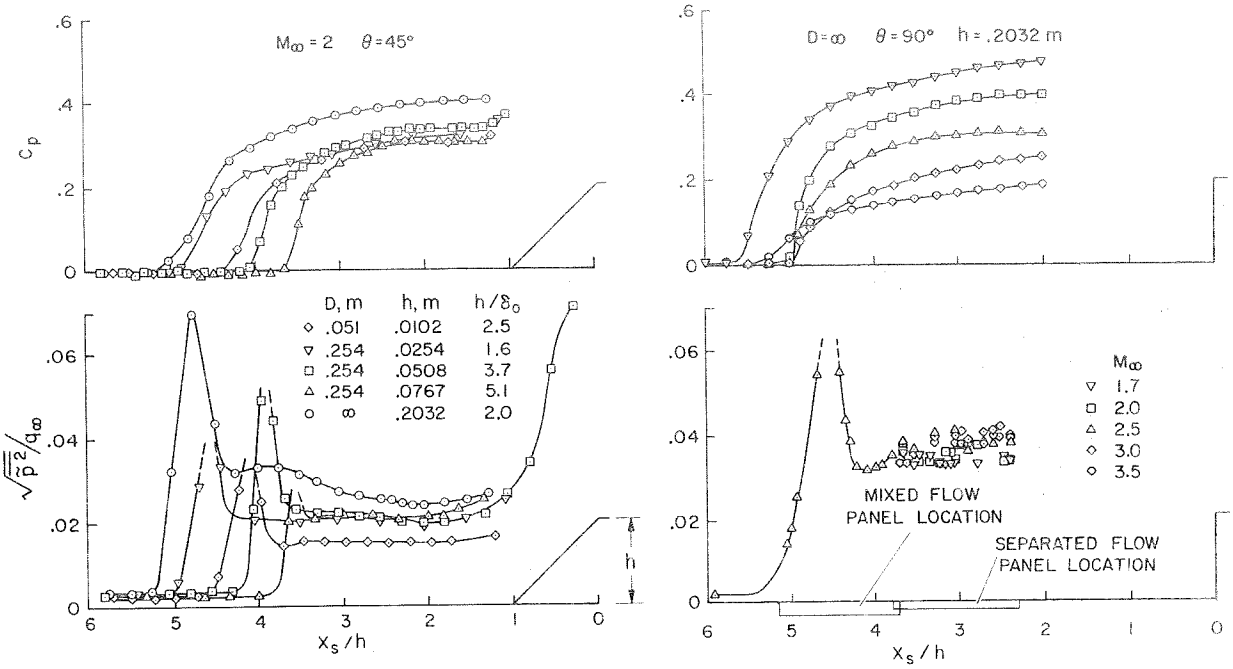

a) Effect of diameter and frustum/wedge height.

b) Effect of Mach number.

Figure 4. Longitudinal distribution of steady and fluctuating static pressures in region of separated flow.

with the higher static pressures in the separated flow region on the two-dimensional model. Generally, the Mach number effects on the broadband pressure fluctuations (Fig. 4(b)) in the separated flow are not significant, however, there is a trend showing a slight increase in intensity with increasing Mach number.

2.2 Power Spectral Densities

Power spectra representative of pressure fluctuations in the vicinity of supersonic separated flow are shown in Fig. 5. The curves show the distinct differences in shapes and mean-square amplitudes that distinguish separated flow spectra from spectra measured in regions of the nearby shock wave and attached turbulent boundary layer. Shock spectra are characterized by a very steep slope and high intensities at low frequencies. The lowest frequencies in these data are 10 Hz. The separated-flow spectra were at least one decade lower than the shock spectra at low frequencies. Having a less steep slope, however, the separated-flow spectra crossed the shock spectra, and were the highest spectral intensities obtained at intermediate and high frequencies. The power spectra of the pressure fluctuations beneath the attached boundary layer were more than two decades lower than the separated-flow spectra at low frequencies. Although all the spectra appear to be converging toward a common level and slope at higher frequencies, there was still at least one decade difference between the attached and separated flow spectra at the highest frequencies of this investigation. The spectra labeled "intermittent shock" illustrate the effect of an intermittent excursion of the shock to the maximum limit of its upstream oscillation. Only the very low frequency components of the pressure fluctuations are increased in intensity, while the intermediate and high frequencies retain the intensities of the attached boundary layer.

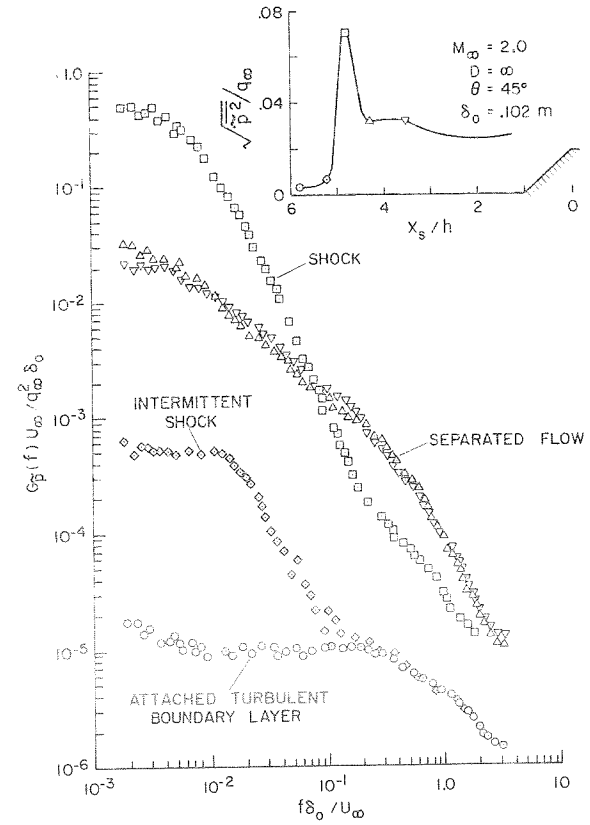

Figure 5. Typical power spectra of pressure fluctuations underlying supersonic flow.

2.2.1 Nondimensionalization of Power Spectra

Many geometric and flow parameters were considered for the nondimensionalization of pressure fluctuations when presented in the frequency domain. Various combinations of length and velocity were applied to the generally accepted reduced frequency parameter having the form (frequency × length)/velocity. The mean-square amplitudes per unit reduced frequency were nondimensionalized by (pressure)$^{-2}$. Some of the

reduced-frequency parameters investigated were: $f\delta_o/U_\infty$, $f\delta_o^*/U_\infty$, fS_s/U, $f(S_s - x_s)/U$, $f\delta/U$, and $f\delta/U_\infty$.

It became evident early in the investigation that there was no reduced-frequency or spectral-density parameter that was the most effective for scaling the data from the many models, particularly for separated flow, for the full range of frequencies considered. (Certain characteristics of the pressure fluctuations were found to be different within different ranges of reduced frequencies.) It was clear however, that the parameters $f\delta/U$ and $f(S_s - x_s)U$ involving local boundary-layer thickness or flow-separation dimensions and local velocity were best for scaling frequencies in separated flow. In this paper, since both attached and separated boundary layers are considered, the nondimensionalization of spectra are illustrated in terms of $f\delta/U$. The data used for the response computation are also presented in terms of $f\delta/U_\infty$ since the local velocity in the separated region is frequently not available and also since differences in scaling with U vs U_∞ are relatively minor. Also minor differences were found in the effectiveness of free-stream versus local dynamic pressure for scaling the spectral density; therefore, the choice has been made in favor of the more conveniently available q_∞.

Local boundary layer thicknesses used for scaling the pressure-fluctuation data were based on measurements of boundary-layer profiles for all the attached-flow test cases and on profiles measured within the separated flow region on the d = 0.254 m, h = 0.0508 m, θ = 45° model. The separated-flow boundary layer measurements are shown in Fig. 6 to illustrate that the boundary-layer growth rearward from the separation point was sufficiently linear to allow a simple linear interpolation of local boundary-layer thickness. Local boundary-layer thicknesses in separated flow were therefore estimated for all the models from the relationship $\delta = \delta_o + h\,(S_s - x_s)/S_s$.

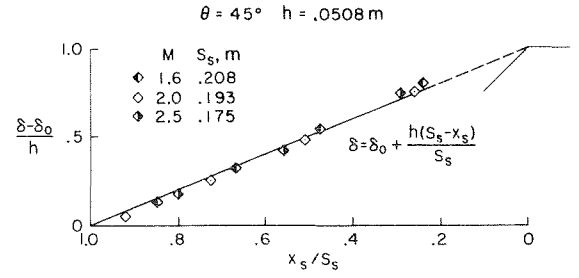

Figure 6. Boundary-layer thickness of separated flow.

Typical scaling of spectral measurements obtained on the different models at M = 2.0 is illustrated in Fig. 7. The spectrum selected for each model represents an approximate mean of from 10 to 20 measurements, and in most of the separated flow cases the mean spectrum was obtained near the center of the separated flow region. The closeness of fit of the spectra scaled by the reduced frequency parameter $f\delta/U$ (Fig. 7) illustrates about the best attainable collapse of data. Most of the separated flow results fit within a factor-of-two spread on the mean-squared spectral density scale. This is considered a good fit of random dynamic data obtained on so many different models, and indicates relative independence of the pressure-fluctuation characteristics on geometry.

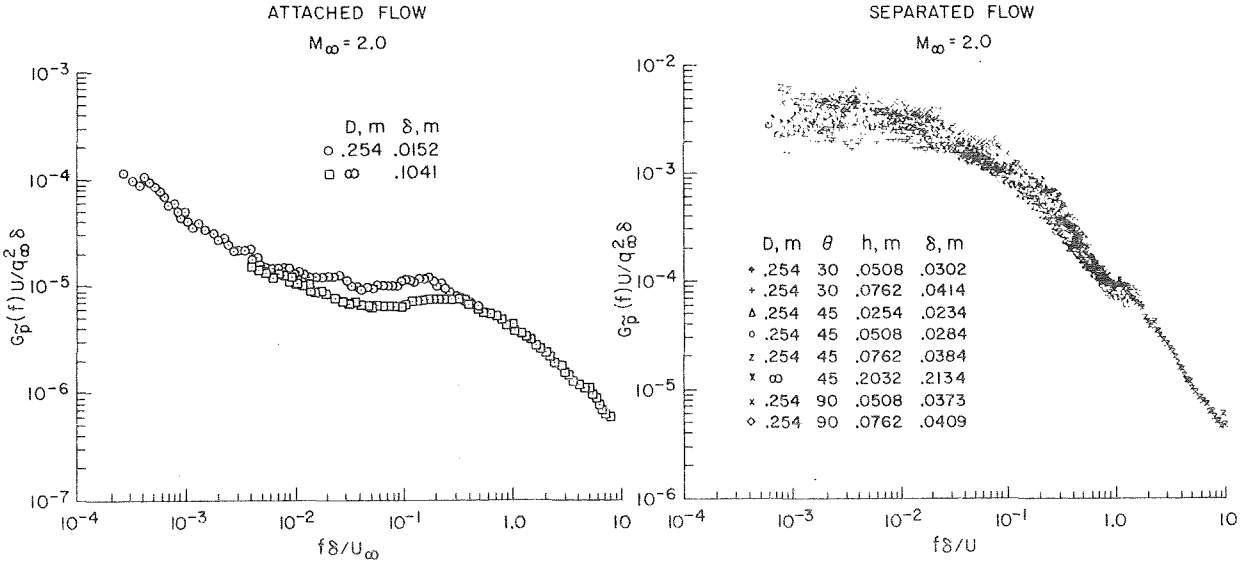

Figure 7. Scaling of power spectra.

2.2.2 Mach Number Effects of Power Spectra

The variation of power spectra in attached and separated flows between Mach numbers of 1.6 and 3.5 is shown in Fig. 8. Each of these spectra represents an average of from 10 to 20 spectra measured on a rigid plate installed in the "panel-response" test fixture in the walls of the Ames 9- by 7-foot SWT and 8- by 7-foot SWT. These data form the basis of the representation of the excitation spectrum used for panel response calculations. Note that the data are nondimensionalized by free-stream velocity.

The power spectra for attached flow generally are very similar for all Mach numbers with the exception of a slightly lower measured spectrum at M = 3. There is a reasonably consistent trend at low reduced frequencies,

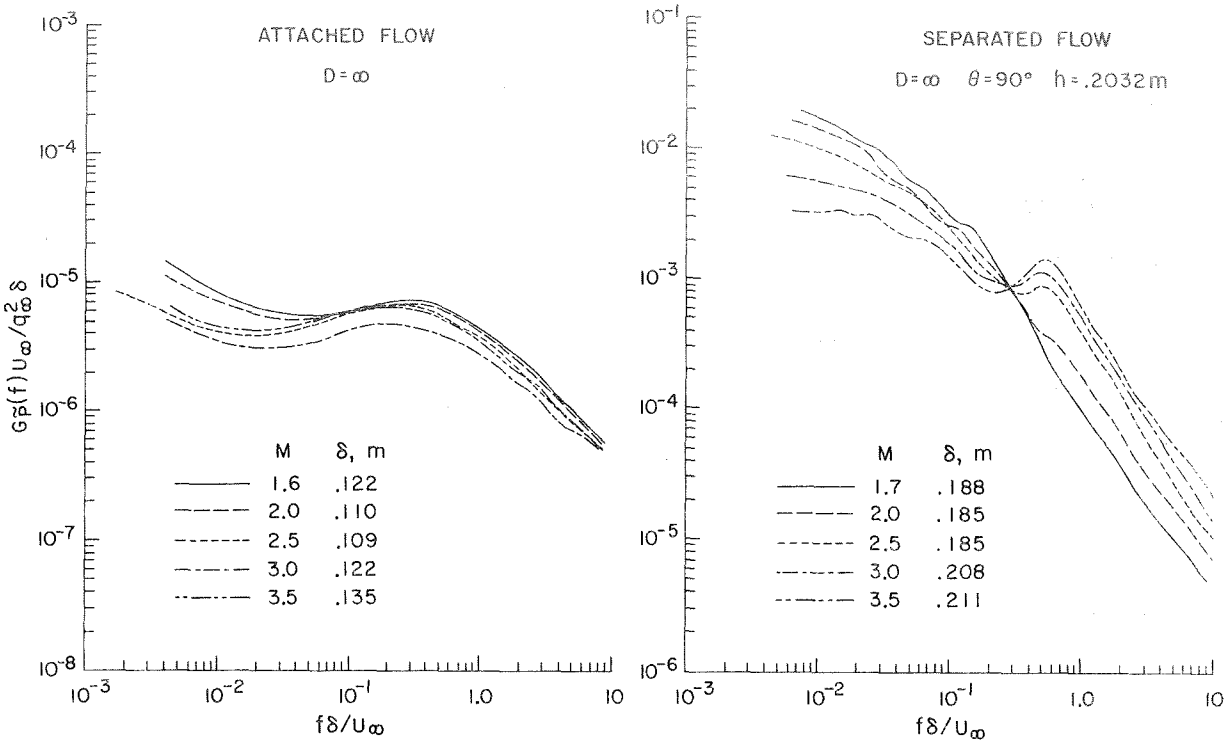

Figure 8. Variation of power spectra with Mach number.

$f\delta/U_\infty < 0.05$, that indicates a reduction in spectrum level with increasing Mach number. These variations should be taken lightly, however, because of reduced statistical accuracy of analysis at the lower frequencies. In contrast with the attached flow case the power spectra measured in the separated flow show a very consistent variation with Mach number. The spectral levels decrease with increasing Mach number at $f\delta/U_\infty < 0.3$ and increase with increasing Mach number at $f\delta/U_\infty > 0.3$. These results illustrate the separation of frequency regimes at $f\delta/U_\infty = 0.3$. In each regime the pressure fluctuations are dependent upon different phenomena. The surface pressure measurements in the lower frequency region are mainly sensitive to the transmitted fluid fluctuations in the turbulent flow of the separated boundary layer; the radiated energy is negligible. In the higher frequency region, it is believed that the surface pressure fluctuations are strongly influenced by an eddy Mach wave radiation phenomena. This phenomena was investigated by Ffowcs-Williams (ref. 16), and although his results do not apply to the study of surface pressure fluctuations a study currently in progress by Dr. Richard D. Rechtien of the University of Missouri, Rolla, Missouri, (NASA-Ames Grant) indicates a dependence of these data on Mach wave radiation.

2.3 Spatial Correlation of Pressure Fluctuations

Chyu and Hanly (ref. 4) presented some data from this investigation that showed the power and cross spectra and space-time correlations of fluctuating pressures underlying the supersonic attached boundary layer on the 0.254-m diameter ogive cylinder and the separated boundary layer ahead of the 0.0508-m high frustum. Among other things, they investigated the co- and quad-spectral density and coherence as functions of a wave number parameter $f\xi_1/U_c(f)$. Illustrative coherence functions are shown in Fig. 9. The results indicate a similarity between the coherence measurements in attached and separated flow at supersonic Mach numbers, but only if the velocity term is $U_c(f)$. The use of convection velocity instead of free-stream velocity is necessary, since for separated flow, $U_c(f)$ varies significantly with frequency. The general trends of the data are also similar to the subsonic-flow measurements by Bull (ref. 11). It can be seen that the envelope of the coherence functions for various spatial distances ξ_1/δ^* decreases exponentially with increasing frequency, however, the envelope unfortunately represents the coherence only at high frequencies.

Chyu and Au-Yang (ref. 12) used Bull's coherence data to represent the subsonic attached-boundary-layer spatial correlation for application to the response computation. The fact that the coherence functions do not collapse complicates the empirical expression

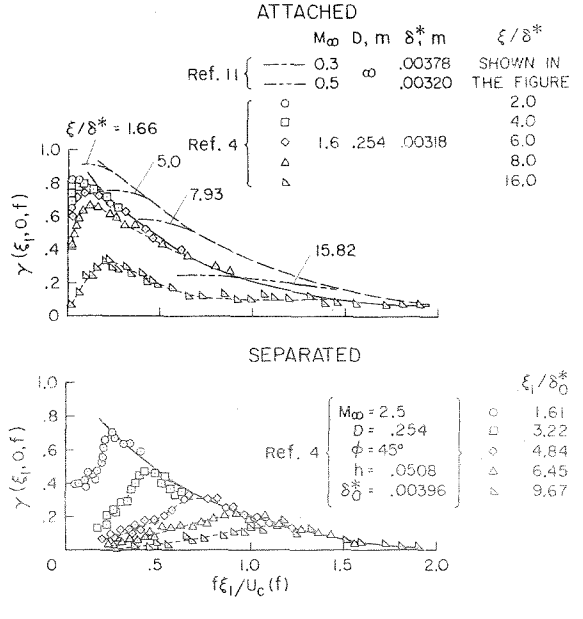

Figure 9. Longitudinal coherence of pressure fluctuations.

of correlation, and therefore, a different approach has more recently been investigated. As suggested by Rechtien the normalized moduli of the cross spectral densities, $|G_p(\xi, f)|_{norm}$, for available or selected transducer spacings have been curve-fitted to the exponential function $|G_p(\xi, f)|_{norm} = e^{-\xi\alpha}$ by the method of least squares to obtain a nondimensional attenuation-coefficient function $\alpha(\xi, f)\delta$. Typical moduli of the cross-spectral densities of the pressure fluctuations in separated flow that were used for the evaluation of the attenuation coefficient are shown in Fig. 10.

Figure 11 shows the attenuation-coefficient function measured in separated flow on the 0.254-m diameter model with the 0.0508-m high 45° frustum shoulder to illustrate its effectiveness of describing spatial correlation. The function is shown to be reasonably independent of the number of moduli, the transducer spacing, or the reference locations involved in the curve fitting. These results indicate that the flow is relatively homogeneous within the limited area of the separated flow region where the measurements were obtained. It appears that the attenuation coefficients decreased slightly at higher frequencies as the larger transducer spacings were used in the analysis. The variation is considered insignificant, however, in light of the state of the art of the structural part of the problem of predicting response to random turbulence. Attenuation coefficients obtained from transducer arrays oriented longitudinally, diagonally, and laterally to the free-stream flow indicate that the decay of correlated turbulence was independent of orientation at $f\delta/U < 0.06$. The predominant turbulence is therefore nonconvective at the lower frequencies, and contours of equal spatial correlation would be circular. At $f\delta/U > 0.06$ the attenuation coefficients were progressively lower as the angularity of the transducer orientation changed from lateral to longitudinal, indicating extended correlation in the direction of free-stream flow.

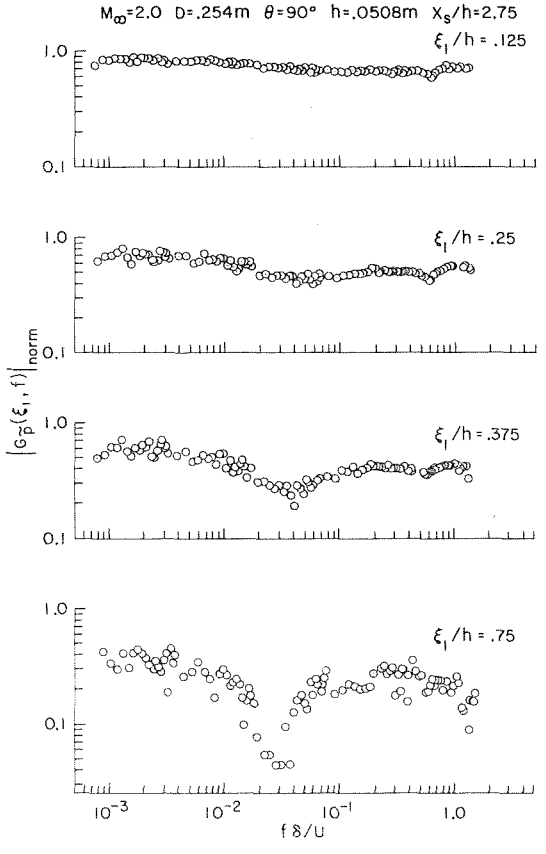

Figure 10. Variation of normalized cross spectra with longitudinal spacing of transducers in separated flow.

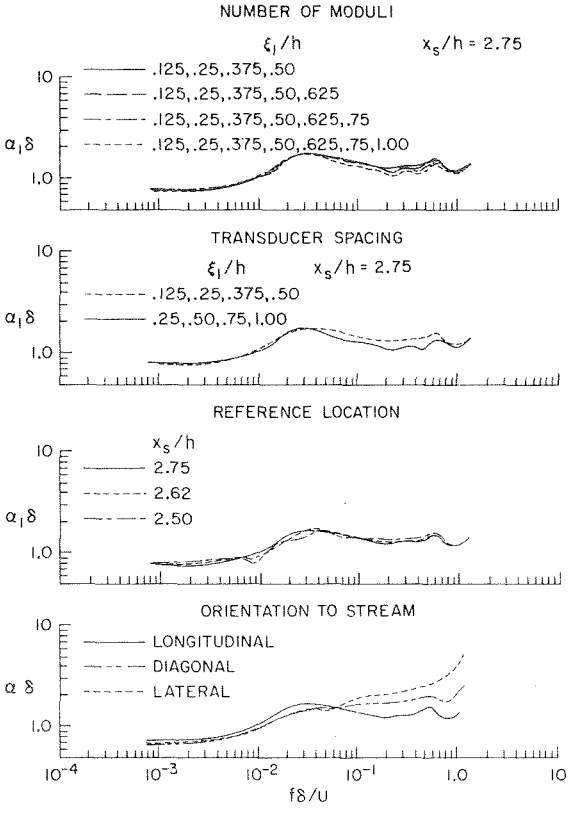

Figure 11. Attenuation coefficients measured on the 0.254-m diameter model in the region of separated flow, h = 0.0508 m, $\phi = 45°$.

A comparison of longitudinal attenuation coefficient functions obtained on the different models in separated flow is shown in Fig. 12 to illustrate the effectiveness of $\alpha\delta$ for scaling for separated flow. The results indicate that the nondimensionalized attenuation coefficients were in relatively good agreement, showing a total spread between all the curves of generally less than a factor of two.

Typical longitudinal attenuation coefficients at Mach numbers from 1.6 to 3.5 are shown in Fig. 13 for both attached and separated flow on the wind tunnel walls. As with the spectra (Fig. 8) the separated flow data show a more consistent variation with Mach number than the attached flow data, particularly at the lower frequencies. The results show that the pressure fluctuations in attached flow were most highly correlated at $f\delta/U_\infty \approx 0.4$; whereas, in separated flow the maximum correlation occurred at the lowest frequencies. The dips in separated flow $\alpha_1\delta$ curves in the frequency range $0.3 < f\delta/U_\infty < 1.3$ indicate increased correlation that is believed to result from the Mach wave radiation phenomena discussed in connection with the observed Mach number effects on power spectra.

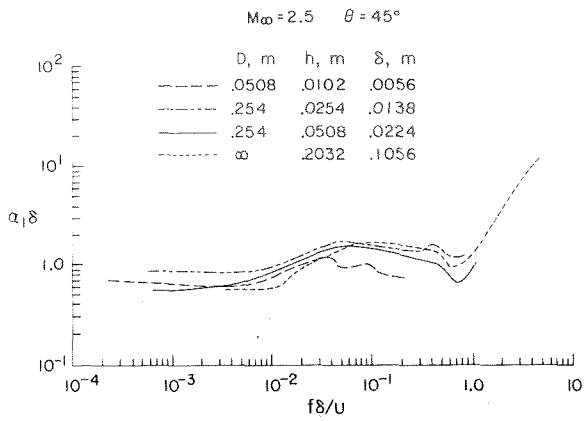

Figure 12. Scaling of attenuation coefficients.

2.4 Phase Angles of Cross Spectra

The convection of turbulence in attached and separated boundary layers results in an angle of phase between spatially correlated components of pressure. Since this phase angle can result in matching of panel flexural waves and pressure waves and thus cause an enhancement of response, it is necessary that it be accounted for in response computations. Convection of the surface-pressure fluctuations can be studied directly in terms of convection velocities or in terms of the phase angles of the cross spectra. The broadband convection velocity derived from space-time correlations is the most convenient description of convection characteristics for attached flow, but Chyu and Hanly (ref. 4) showed that it is inappropriate for separated flow since convection velocities vary with frequency.

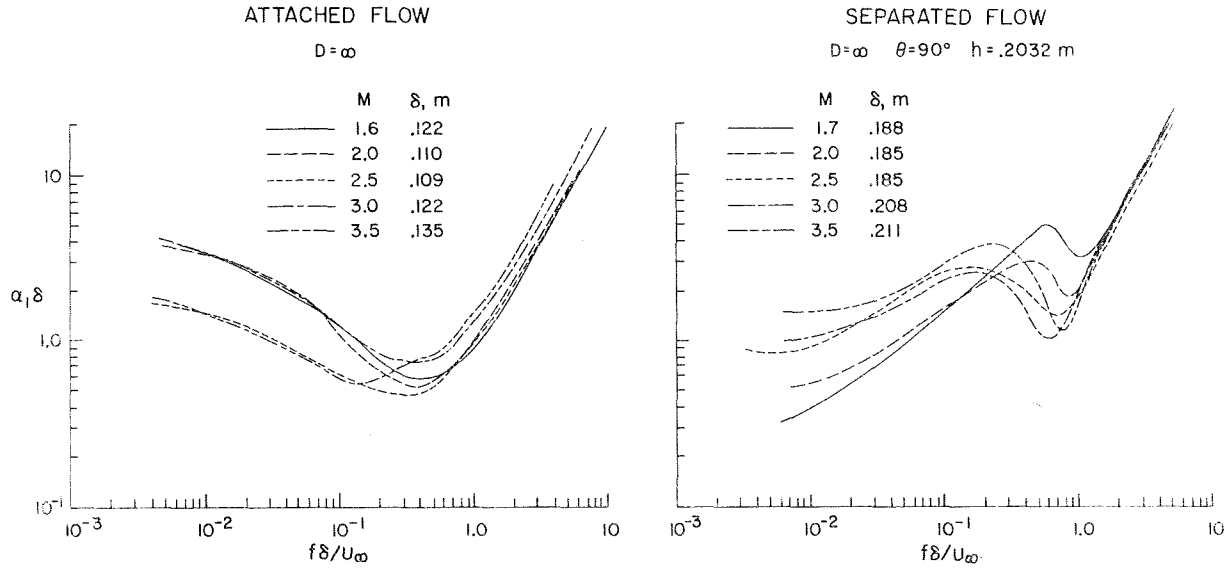

Figure 13. Effect of Mach number on longitudinal attenuation coefficients.

Typical phase angles that result from convection of the turbulence in separated flow are shown in Fig. 14. The data were obtained on the 0.254-m diameter model with axisymmetric flow and show the effects of the angular orientation of a transducer array to the free-stream flow direction. At low frequencies, f < 300 Hz, the phase angles were zero for all angular orientations. A zero phase angle indicates a zero or infinite speed of convection of the pressure fluctuations between two points, as would exist with a stationary pulsating bubble or for normal incidence of an acoustic radiation process. The equivalent of the pulsating bubble could occur if the turbulence is related to fore-and-aft oscillations of the detached shock wave. The phase-angle measurements generally indicate an absence of lateral convection in the separated flow over the full range of frequencies investigated. This result was evidenced by the near zero lateral measurements and by the agreement between longitudinal and diagonal measurements of θ/ξ_1 (phase angle per meter of longitudinal component of transducer spacing).

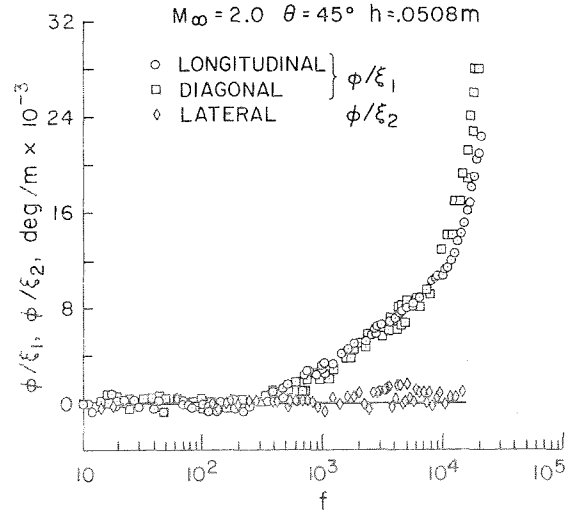

Figure 14. Typical phase angles of cross spectra of pressure fluctuations underlying separated flow.

2.5 Narrow-Band Convection Velocities

When significant phase angles are measured, they can be converted to convection velocities, as defined by $360\, f(\xi/\phi)$, and thus reveal the narrow-band convection characteristics of the turbulence. Figure 15 shows that on the 0.254-m diameter model, the convection velocities of the pressure field in separated flow varied from a minimum of approximately 0.2 U at $f\delta/U \approx 0.6$ to a plateau

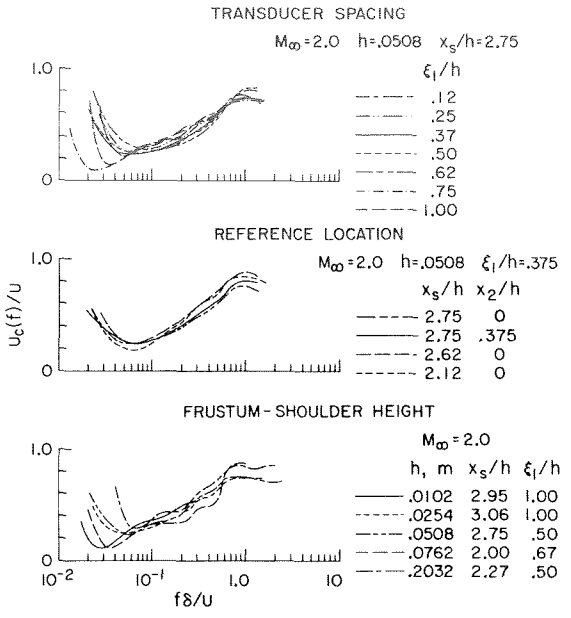

Figure 15. Typical narrow-band convection velocities.

near 0.8 U at $f\delta/U \approx 0.8$. The variation of convection speed with frequency infers that the predominant turbulence at different frequencies between $0.03 < f\delta/U < 0.8$ is generated at different levels of the boundary layer ranging from slightly above the zero velocity line to the free-shear layer. Upstream convection was not detected between points within the separated flow region. The turbulent eddies generated in the reverse flow region apparently contribute little to the wall-pressure fluctuations. With the exception of the low frequency region of $f\delta/U < 0.06$, the convection velocities were relatively unaffected by transducer spacing or reference location. It is also shown that they can be effectively scaled by the reduced frequency parameter $f\delta/U$.

Representative narrow-band convection velocities in attached and separated flows on the walls of the 9- by 7-foot SWT and 8- by 7-foot SWT at the location of the panel response test fixture are shown in Fig. 16. It can be seen that for attached flow there was no significant variation in the ratio of convection velocity to free-stream velocity ($U_c(f)/U_\infty \approx 0.75$) with frequency or Mach number. The variation of convection velocity with frequency in separated flow was previously discussed in connection with Fig. 15. This variation with frequency was relatively unaffected by Mach number at $f\delta/U_\infty < 0.6$. The plateau values of nearly constant U_c/U_∞ at $f\delta/U_\infty > 1.0$, however, varied inversely with Mach number (with the exception of the $M_\infty = 3.5$ data) so that the absolute convection velocity, U_c, was nearly constant. The convection velocity in this plateau region varied from approximately 354 m/sec (1150 fps) at $M_\infty = 1.7$ to 366 m/sec (1200 fps) at $M_\infty = 3.0$. The reduced frequencies where the beginning of the plateau occurs can be identified with changes in the characteristics of the power spectra and attenuation coefficients.

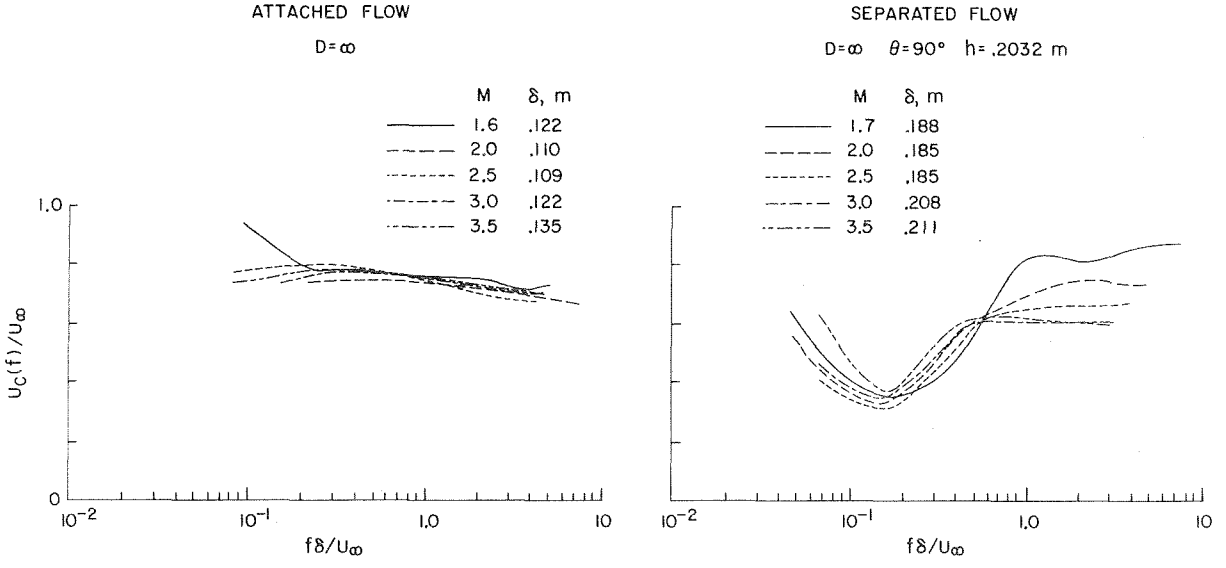

Figure 16. Variation of narrow-band convection velocities with Mach number.

2.6 Representation of Surface-Pressure Fluctuations

The fundamental information needed to describe the excitation of a structure underlying a turbulent flow is the cross spectral density of the fluctuating pressures.

In a homogeneous turbulence the cross spectra can be expressed in the form

$$\frac{S_{\tilde{p}}(\xi_1, \xi_2, \omega)}{S_{\tilde{p}}(\omega)} = \left|\rho_{\tilde{p}}(\xi_1, \xi_2, \omega)\right| e^{-i\omega\xi_1/U_c} \tag{1}$$

where $\left|\rho_{\tilde{p}}(\xi_1, \xi_2, \omega)\right|$ is the cross correlation coefficient between two points separated by distance ξ_1 and ξ_2 in the x_1 and x_2 directions. Experimental data have also shown that the correlation coefficient can be separated in coordinates as follows:

$$\left|\rho_{\tilde{p}}(\xi_1, \xi_2, \omega)\right| = \left|\rho_{\tilde{p}}(\xi_1, 0, \omega)\right| \left|\rho_{\tilde{p}}(0, \xi_2, \omega)\right| \tag{2}$$

where $\left|\rho_{\widetilde{p}}(\xi_1, 0, \omega)\right| = \exp\left[-\alpha_1 \xi_1\right]$ and $\left|\rho_{\widetilde{p}}(0, \xi_2, \omega)\right| = \exp\left[-\alpha_2 \xi_2\right]$.

The convection velocity U_c is related to the phase angle ϕ of the cross spectral density of the fluctuating pressure by $U_c = 360\, f\xi_1/\phi$. For this investigation, it has been chosen to represent U_c in terms of ϕ since U_c varies significantly with f for separated flow and since $\phi \to 0°$, $U_c \to \infty$. It should also be noted that ϕ/ξ_1 is an independent function of f and is therefore not scaled by a reduced frequency parameter.

To derive expressions that represent the selected functions used to describe the fluctuating pressures in supersonic attached and separated turbulent boundary layers, the large amount of experimental data previously discussed have been averaged at each test Mach number (1.6, 2.0, 2.5, 3.0, 3.5) and approximate means of the envelopes of these data have been curve-fitted as shown in Fig. 17.

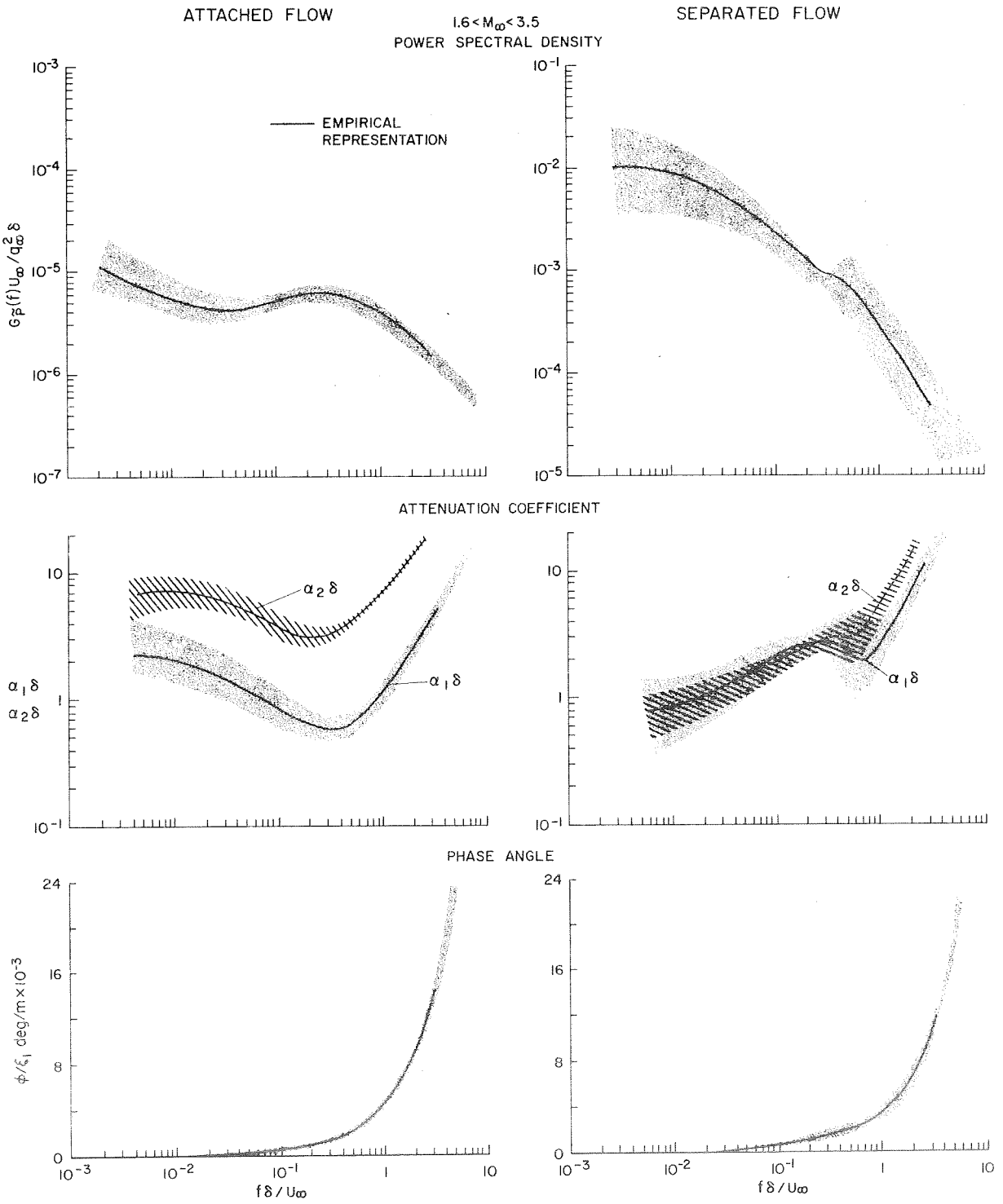

Figure 17. Representation of surface-pressure fluctuations.

The empirical formulae that express the power spectrum, attenuation coefficients, and phase angles for attached and separated flows are as follows:

a) For attached flow

Power Spectrum

$$G_{\tilde{p}} U_\infty / q_\infty^2 \, \delta = \exp \{-12.470 - 0.639x - 0.269x^2 + 0.015x^3 + 0.017x^4 + 0.002x^5\} \tag{3}$$

Attenuation Coefficients

$$\alpha_1 \delta = \exp \{0.060 + 0.941x + 0.380x^2 - 0.023x^3 - 0.020x^4 - 0.002x^5\} \tag{4}$$

$$\alpha_2 \delta = \exp \{2.163 + 1.291x + 0.262x^2 - 0.132x^3 - 0.043x^4 - 0.0033x^5\} \tag{5}$$

Phase Angle

$$\phi / \xi_1 = 39.37 \{115.14 + 131.99x + 69.89x^2 + 18.84x^3 + 2.44x^4 + 0.12x^5\} \text{ deg/m} \tag{6}$$

b) For separated flow

Power Spectrum

$$G_{\tilde{p}} U_\infty / q_\infty^2 \, \delta = \exp \{-8.094 - 1.239x - 0.295x^2 - 0.090x^3 - 0.014x^4 - 0.001x^5\} \tag{7}$$

Attenuation Coefficients

$$\alpha_1 \delta = \exp \{1.031 + 0.666x + 0.645x^2 + 0.270x^3 + 0.043x^4 + 0.002x^5\} \tag{8}$$

$$\alpha_2 \delta = \exp \{1.797 + 1.239x + 0.536x^2 + 0.122x^3 + 0.010x^4\} \tag{9}$$

Phase Angle

$$\phi / \xi_1 = 39.37 \{90.54 + 89.28x + 50.47x^2 + 15.69x^3 + 2.32x^4 + 0.13x^5\} \tag{10}$$

Where for both a) and b) above: $x = \log_e (f\delta / U_\infty)$

3. RESPONSE OF FLAT CLAMPED-EDGE PANELS

3.1 Method of Analysis

The displacement $w(\underline{x}, t)$ of a vibrating panel (Fig. 18), is assumed to obey the classical thin plate equation

$$\mu \ddot{w} + c\dot{w} + B\nabla^4 w = \tilde{p}(\underline{x}, t) \tag{11}$$

where μ and B are constants and independent in the present analysis. It is assumed further that $w(\underline{x}, t)$ can be expanded in terms of $\psi_\alpha(\underline{x})$ as follows:

$$w(\underline{x}, t) = \sum_\alpha q_\alpha(t) \psi_\alpha(\underline{x}) \tag{12}$$

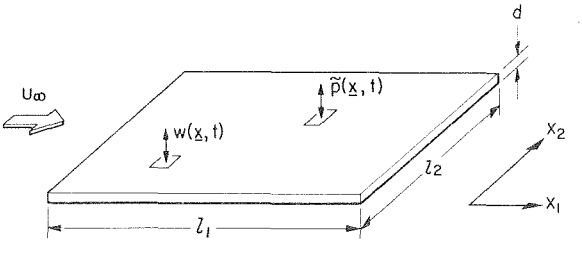

Figure 18. Schematic of a panel with flow excitation.

Here ψ_α is assumed to be properly normalized and separable in coordinates, i.e.,

$$\int_A \psi_\alpha(\underline{x}) \, \psi_\beta(\underline{x}) \, dx = \delta_{\alpha\beta} \tag{13}$$

and

$$\psi_\alpha(\underline{x}) = \psi_m(x_1) \, \psi_n(x_2) \tag{14}$$

It can be shown that for a panel with clamped edges ψ_m takes on different forms according to whether m is even or odd:

a) If m is odd,

$$\psi_m(x_i) = \frac{1}{A_m\sqrt{\ell_i}} \cos\gamma_m\left(\frac{x_i}{\ell_i} - \frac{1}{2}\right) + K_m \cosh\gamma_m\left(\frac{x_i}{\ell_i} - \frac{1}{2}\right) \tag{15}$$

where γ_m are the roots of the equation

$$\tan\frac{\gamma_m}{2} + \tanh\frac{\gamma_m}{2} = 0$$

and

$$K_m = \frac{\sin(\gamma_m/2)}{\sinh(\gamma_m/2)}$$

b) If m is even,

$$\psi_m(x_i) = \frac{1}{A_m\sqrt{\ell_i}} \sin\gamma_m\left(\frac{x_i}{\ell_i} - \frac{1}{2}\right) + K_m \sinh\left(\frac{x_i}{\ell_i} - \frac{1}{2}\right) \tag{16}$$

where γ_m are the roots of the equation

$$\tan\frac{\gamma_m}{2} - \tanh\frac{\gamma_m}{2} = 0$$

By using the orthogonality condition of the mode-shape function, the normalizing factors A_m can be found to be

$$A_m = \frac{\sqrt{2}\,\gamma_m}{Z_m}$$

where

$$Z_m = \gamma_m + \sin\gamma_m + K_m^2(\sinh\gamma_m + \gamma_m) \quad \text{if m is odd}$$

$$= \gamma_m - \sin\gamma_m + K_m^2(\sinh\gamma_m - \gamma_m) \quad \text{if m is even}$$

The generalized coordinates $q_\alpha(t)$ satisfies the Lagrange equation

$$m_\alpha\ddot{q}_\alpha(t) + C_\alpha\dot{q}_\alpha(t) + K_\alpha q_\alpha(t) = f_\alpha(t) \tag{17}$$

where the generalized mass

$$m_\alpha = \mu\int_A \psi_\alpha^2(\underline{x})d\underline{x} = \mu$$

$$K_\alpha = m\omega_\alpha^2$$

$$f_\alpha(t) = \int_A \tilde{p}(\underline{x}, t)\psi_\alpha(\underline{x})d\underline{x}$$

and

$$C_\alpha = \frac{K_\alpha \nu_\alpha}{\omega}$$

here ν_α is the combined loss factor for both structural and viscous damping. The present state of art requires that ν_α must be measured experimentally. The Fourier transform of the Lagrange Eq. (17) takes the form

$$Q_\alpha(\omega) = H_\alpha(\omega)F_\alpha(\omega) \tag{18}$$

where

$$H_\alpha(\omega) = \frac{1}{m_\alpha\{(\omega_\alpha^2 - \omega^2) + i\nu_\alpha\omega^2\}} \tag{19}$$

Equations (12) and (18) together give

$$W(\underline{x}, \omega) = \sum_\alpha H_\alpha(\omega) F_\alpha(\omega) \psi_\alpha(\underline{x}) \tag{20}$$

The displacement power-spectral density is related to $W_T(\underline{x}, \omega)$ by

$$S_d(\underline{x}, \omega) = \lim_{T\to\infty} \frac{\pi}{T} W_T^*(\underline{x}, \omega)\, W_T(\underline{x}, \omega) \tag{21}$$

where W_T is the truncated Fourier transform of w. Equations (17), (18), (20), and (21) together give the displacement power spectral density in the form:

$$S_d(\underline{y}, f) = S_{\tilde{p}}(f) \sum_\alpha \bar{\psi}_\alpha^2(\underline{y}) \left|H_\alpha(\omega)\right|^2 j_{mm}(F_1) j'_{nn}(F_2)$$

$$+ S_{\tilde{p}}(f) \sum_{\alpha\neq\beta} \frac{\bar{\psi}_\alpha(\underline{y})\bar{\psi}_\beta(\underline{y}) j'_{ns}(F_2)\left[g_{\alpha\beta} j_{mr}(F_1) + h_{\alpha\beta} k_{mr}(F_1)\right]}{m_\alpha m_\beta (g_{\alpha\beta}^2 + h_{\alpha\beta}^2)} \tag{22}$$

where

$$g_{\alpha\beta} = (\omega_\alpha^2 - \omega^2)(\omega_\beta^2 - \omega^2) + \nu_\alpha\nu_\beta\omega_\alpha^2\omega_\beta^2$$

$$h_{\alpha\beta} = \nu_\alpha\omega_\alpha^2(\omega_\alpha^2 - \omega^2) - \nu_\alpha\omega_\beta^2(\omega_\alpha^2 - \omega^2)$$

$$j_{mr}(F_1) = 2\int_0^1\int_0^{y_1''} \bar{\psi}_m(y_1')\bar{\psi}_r(y_1'') \left|\rho_{\tilde{p}}\left(\eta_1, 0, \frac{\pi F_1}{2}\right)\right| \cos\frac{\pi F_1\eta_1}{2}\, dy_1' dy_1'' \quad \text{if m + r even}$$

$$= 0 \quad \text{if m + r odd} \tag{23}$$

$$j'_{ns}(F_2) = 2\int_0^1\int_0^{y_2''} \bar{\psi}_n(y_2')\psi_s(y_2'') \left|\rho_{\tilde{p}}\left(0, \eta_2, \frac{\pi F_2}{2}\right)\right| dy_2' dy_2'' \quad \text{if n + s even}$$

$$= 0 \quad \text{if n + s odd} \tag{24}$$

and

$$k_{mr}(F_1) = 2\int_0^1\int_0^{y_1''} \bar{\psi}_m(y_1')\bar{\psi}_r(y_1'') \left|\rho_{\tilde{p}}\left(\eta_1, 0, \frac{\pi F_1}{2}\right)\right| \sin\frac{\pi F_1\eta_1}{2}\, dy_1' dy_1'' \quad \text{if m + r odd}$$

$$= 0 \quad \text{if m + r even} \tag{25}$$

Here $\bar{\psi}_m(y)$ are the normalized mode-shape functions, expressed by Eqs. (15) and (16) with ℓ replaced by unity. The physical significance of the structural acceptances j_{mr} is discussed by Ref. 12. The pressure correlation coefficients $\rho_{\tilde{p}}$ are experimentally shown to be related to the cross spectral density of the fluctuating pressure in a homogeneous turbulence and can be expressed by

$$\frac{S_{\tilde{p}}(\xi_1, \xi_2, \omega)}{S_{\tilde{p}}(\omega)} = \left|\rho_{\tilde{p}}(\xi_1, 0, \omega)\right| \left|\rho_{\tilde{p}}(0, \xi_2, \omega)\right| e^{-i\omega\xi_1/U_c} \tag{26}$$

The strains in the x_1 and x_2 directions of a rectangular plate are related to the displacement w by

$$\epsilon_1 = \frac{(1/2)d}{1-\nu^2}\left(\frac{1}{r_1} + \nu\frac{1}{r_2}\right), \qquad \epsilon_2 = \frac{(1/2)d}{1-\nu^2}\left(\frac{1}{r_2} + \nu\frac{1}{r_1}\right) \tag{27}$$

where

$$\frac{1}{r_1} = -\frac{\partial^2 w}{\partial x_1^2}, \quad \frac{1}{r_2} = -\frac{\partial^2 w}{\partial x_2^2}$$

are the curvatures in x_1 and x_2 directions. The strain spectrum can be obtained by

$$S_{\epsilon_i}(\underline{x}, \omega) = \lim_{T\to\infty} \frac{\pi}{T} E^*_{i_T}(\underline{x}, \omega) E_{i_T}(\underline{x}, \omega) \tag{28}$$

where E_{i_T} is the truncated Fourier transform of ϵ_i in Eq. (27), and can be expressed by

$$E_1(\underline{x}, \omega) = \sum_\alpha H_\alpha(\omega) F_\alpha(\omega) \Phi_1^\alpha$$

and (29)

$$E_2(\underline{x}, \omega) = \sum_\alpha H_\alpha(\omega) F_\alpha(\omega) \Phi_2^\alpha$$

where

$$\Phi_1^\alpha = \frac{(1/2)d}{1-\nu^2}\left(\frac{\partial^2 \psi_\alpha}{\partial x_1^2} + \nu \frac{\partial^2 \psi_\alpha}{\partial x_2^2}\right)$$

$$\Phi_2^\alpha = \frac{(1/2)d}{1-\nu^2}\left(\frac{\partial^2 \psi_\alpha}{\partial^2 x_2^2} + \nu \frac{\partial^2 \psi_\alpha}{\partial x_1^2}\right) \tag{30}$$

Equations (28-30) together with the expression for ψ in Eqs. (15) and (16) give the strain power spectrum

$$S_{\epsilon_i}(\underline{x}, f) = A S_{\tilde{p}}(f) \sum_\alpha [\Phi_i^\alpha(\underline{x})]^2 \left|H_\alpha(f)\right|^2 j_{mm}(F_1) j'_{nn}(F_2)$$

$$+ 2 A S_{\tilde{p}}(f) \sum_{\alpha\neq\beta} \frac{\Phi_i^\alpha(\underline{x})\, \Phi_i^\beta(\underline{x})\, j'_{ns}(F_2) \left[g_{\alpha\beta} j_{mr}(F_1) + h_{\alpha\beta} k_{mr}(F_1)\right]}{m_\alpha m_\beta (g_{\alpha\beta}^2 + h_{\alpha\beta}^2)} \tag{31}$$

3.2 Response Measurements and Computations

As briefly described in the introduction, tests have been conducted to measure the displacement and strain response of several panels of different lengths, widths, and thicknesses in supersonic attached and separated flows and in mixed flow with a shock wave positioned on the panels. The response tests of the total input-response investigation have only recently been completed and therefore the following results are somewhat preliminary. All the panels tested were constructed of magnesium having the following properties:

$$E = 4.48\times10^{10}\ \text{N/m}^2$$

$$\rho = 1780\ \text{Kg/m}^3$$

$$\nu = 0.35$$

The first panels selected for analysis had the same dimensions with $\ell_1 = 0.3048$ m, $\ell_2 = 0.2286$ m, $\ell_1/\ell_2 = 4/3$, but two different thicknesses d = 0.00118 m and d = 0.00235 m.

It was recognized prior to the tests that the installation of strain gages on the panels could affect the stiffness and symmetry of response and therefore could compromise the comparison between measurements and computations. Since strain is a key element in fatigue, however, it was considered more important to include the strain gages to verify the strain computations. It would have been desirable to conduct separate displacement response tests, but this was economically impractical.

3.2.1 Systems Damping

In Eq. (19) ν_α is the combined loss factor for the complete structural airstream system. The loss factor therefore takes into account the effect of hysteretic damping as well as viscous damping. The latter includes the interaction of panel motion on the flow field within and outside the boundary layer, and the effect of acoustical radiation

into the interior of the structure (cavity) and into the exterior flow field. Although the development (by Dowell, ref. 17) of an analytical method for the determination of the aerodynamic damping part of the loss factor is in progress, the present state of art requires that ν_{a_y} must be estimated from experience or measured experimentally.

The loss factors used for the computations of panel response as presented in this paper have been measured from the autocorrelations of the response-time histories for the specific panels of interest. Representative loss-factor measurements for a 0.3048-m long, 0.2286-m wide by 0.00235-m thick magnesium panel are shown in Fig. 19 for both attached and separated flows. The results indicate that only the damping of the first mode is significantly higher than the damping of all other modes. The first mode damping was slightly higher in separated flow than in attached flow, but all other modes were relatively unaffected by the flow condition. The effects of Mach number are not clearly defined although it is evident that the effects are not large for the range of Mach numbers investigated. It is expected that the damping would increase significantly for the attached flow case at $1.6 > M > 1.0$. Muhlstein (ref. 18) has shown total-system-damping measurements in attached flow at Mach numbers between 1.1 and 1.4 that decrease a full decade between M = 1.1 and M = 1.4. His results at M = 1.4, although for a much thinner boundary layer relative to the panel length, are consistent with the results in Fig. 19.

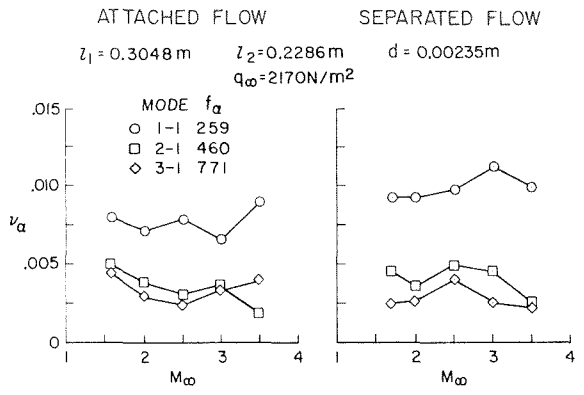

Figure 19. Damping of the panel/air-stream system in terms of loss factor.

3.2.2 Displacement Response

Illustrative measurements and computations of the power-spectral densities of displacement of the 0.00118-m thick panel are shown in Fig. 20 for $M_\infty = 2.5$. Measurements are shown for the probe locations indicated in the inset panel sketches. Corresponding computations for the same locations are shown only for the peak displacements at measured resonance frequencies. The computer program computes the complete spectrum, but this has been omitted to simplify the figures. The results show similar trends between attached and separated flows in the response of most modes as a function of frequency. The first mode predominated the displacement, as would be expected. The relative displacements between attached and separated flows are in the same proportion as the input spectra (Fig. 17). Thus the spatial correlation differences between attached and separated flows have only a subtle influence on the response characteristics. It was originally planned to present longitudinal and lateral acceptances as a function of frequency to illustrate spatial correlation effects, but these results were not available in time to be included in the paper.

The comparison between measured and computed displacement spectral densities at resonance generally shows similar trends with frequency with the computed displacements from about two to ten times higher than the measured displacements. Although the comparative results are considered good and within state of art for random excitation and response phenomena, the anxious and optimistic investigator always hopes for better agreement. The first suspicions are usually directed to searching for computational errors. In this case the computer program and measured spectra have been repeatedly checked. As an example the comparable measured spectra have been obtained by three different analysis systems (2 digital and 1 analog). It is believed that the major differences in computed and measured results are due to the assumptions in the analytical method that the flow field is uniform and homogeneous. An obvious major source of panel response asymmetry is the longitudinal pressure variation on the panel in separated flow (Fig. 4(b)). A slight lateral variation in static pressure was also found on the wind-tunnel wall in the region of the panel for the attached flow case. These effects are somewhat accounted for, but not entirely, by computing the response spectra at the measured natural frequencies. The effects of the strain-gates mounted on the panel are also not accounted for.

3.2.3 Strain Response

Typical measurements and computations of strain response power spectral densities are shown in Fig. 21. The most significant feature of the strains is that the first mode is not the dominant mode as shown in the case for the displacement response. This result is expected since the strains are proportional to the local panel curvature associated with the response mode. In the displacement response the differences between the attached and separated flow are consistent with the difference in the excitation spectra. There is also about the same order of differences between computations and measurements of strain. A few characteristics of the spectra indicate panel distortion and asymmetry of modes as discussed in 3.2.2. An example is the measurement of a significant strain response for the 1-2 mode at the panel center point which should be on a node line.

3.3 Effect of Flow Field on Displacement Response

Comparisons of the displacement responses of two panels ($d = 0.00118$ m and $d = 0.00235$ m), due to the excitations of attached and separated and mixed flows at $M_\infty = 2.5$ are shown in Fig. 22. The results show that the response amplitudes were approximately the same for both the separated flow and mixed flow cases even though the excitation spectra are significantly different in the region of the shock wave (Fig. 5). The increase in mixed flow spectra at $f < 100$ Hz is consistent with the higher excitation spectra at these low frequencies. It is interesting that there was apparently no higher degree of coupling of the shock oscillations in mixed flow with the panel response than occurred in the fully separated flow case. For the mixed flow case, the shock wave was positioned near the center of the panels. The extent of the shock wave oscillations relative to the panel length can be seen in the longitudinal distribution of the fluctuating pressures shown in Fig. 4.

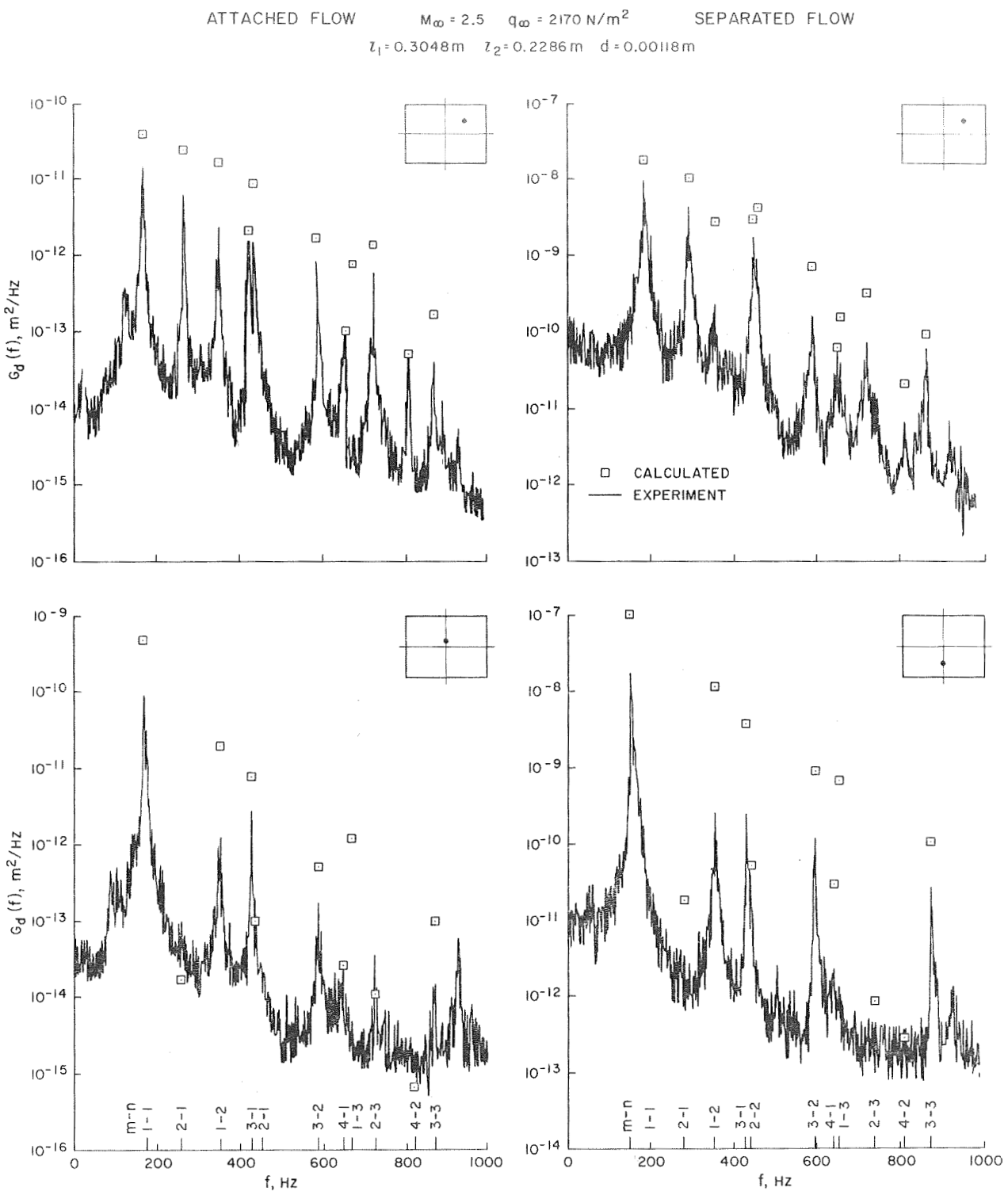

Figure 20. Power spectral densities of displacement response.

The ratio between the attached flow and separated flow response spectra are approximately the same for both panel thicknesses, as would be expected; except that an unexplained broadband mode of vibration occurred at $f \approx 100$ Hz on the $d = 0.00235$ m panel. Significant differences in resonant frequencies can be noted for each of the flow cases. The frequencies also do not scale directly with thickness or with the same scale factor for all modes for the two panel thicknesses. These characteristics can be due to stiffness changes resulting from unsymmetrical loading or midplane stresses due to thermal effects, or due to changes in excitation; however, the distortion of the mode shapes by the unsymmetrical loading on the panels as discussed in 3.2.2 is considered to be the most probable cause.

4. CONCLUDING REMARKS

A large amount of experimental data have been studied to determine the characteristics of surface-pressure fluctuations underlying supersonic attached and separated turbulent boundary layers ($M_\infty = 1.6$ to 3.5). The most effective parameters for making the characteristics dimensionless have been established. Empirical formulae have been derived to represent the nonsteady pressure fields in each of the flow regions. A method of analysis of the amplitude

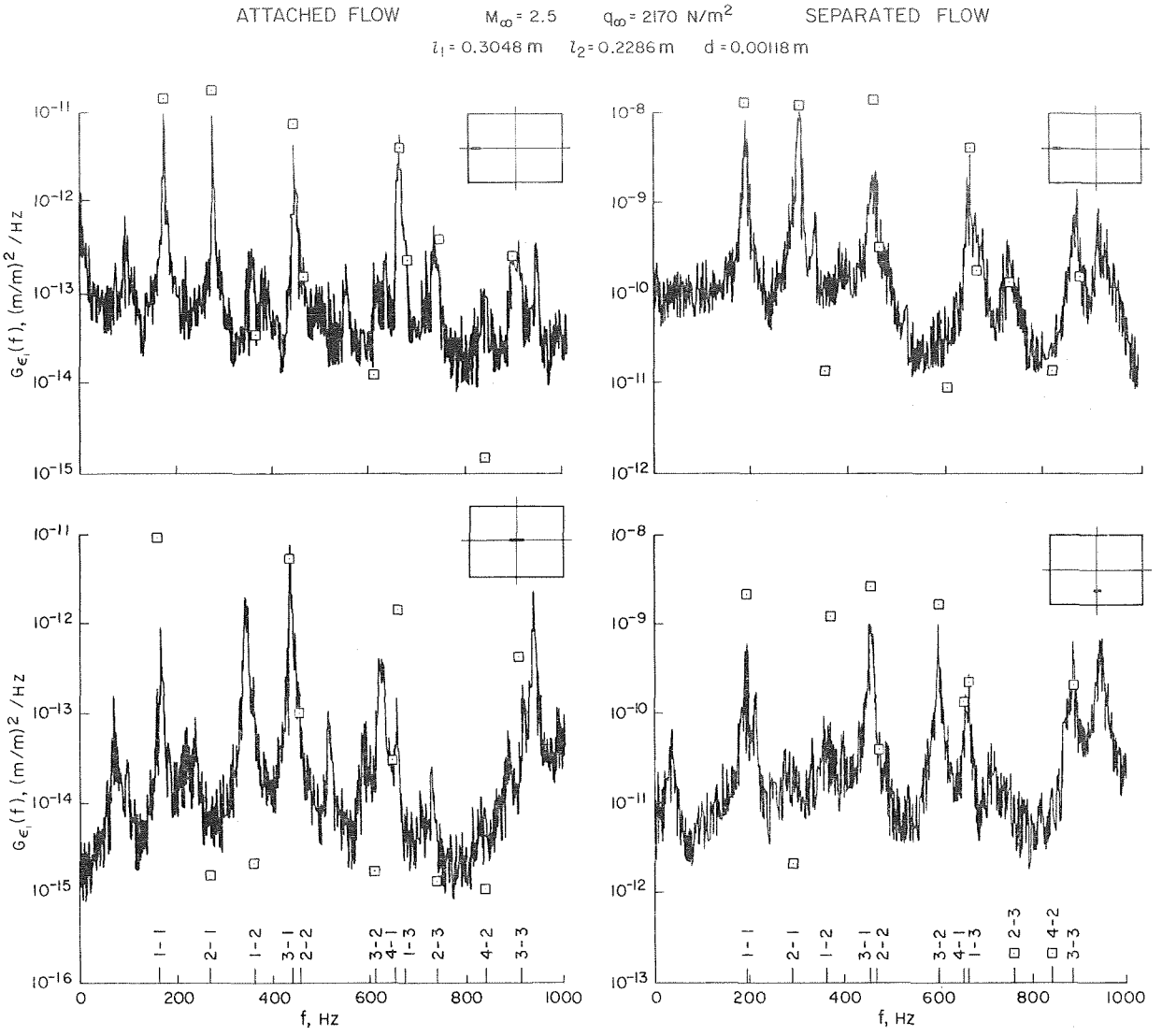

Figure 21. Power spectral densities of stress response.

and strain response of flat clamped-edge panels has also been described, and comparisons have been made between response measurements and computations for panels underlying both the attached and separated flows.

The results of the pressure-fluctuation studies have shown that the turbulence generated within attached or separated flow is relatively homogeneous although some nonuniformities of the fluctuating pressures have been identified. The statistical characteristics that describe the surface fluctuating pressures can be effectively scaled by the reduced frequency parameters $f\delta/U$ or $f\delta/U_\infty$. An attenuation-coefficient function $\alpha\delta$ representing the decaying exponential of the moduli of the cross spectra has been shown to be an appropriate function to describe the spatial correlation of the unsteady pressure fields. Observed irregularities in the shapes of power spectra and attenuation coefficients and convection velocities as a function of frequency can be attributed to changes in the predominant sources of the fluctuating pressures in different frequency zones.

The results of the panel response studies indicate that the method of analysis predicts the relative levels of response of most modes for either attached or separated flow, but generally, over predicts the mean-square amplitudes or strains. It is believed that the differences between computations and measurements result primarily from the assumption in the analysis that the flow fields are uniform and homogeneous, whereas, in the experiments significant nonuniform steady-state loading occurred. The differences in panel response between attached and separated flows are consistent with the approximate three decade change in the excitation spectra. The response of panels to the excitation of mixed flow with an oscillating shock wave near the center of the panels was not significantly different than the response to separated flow even though the excitation in the region of a shock wave has higher amplitude and different frequency content. Indications are that the shock oscillations did not couple to any degree with the panel motions. The damping of panel-airstream system was relatively invariant with Mach number at constant total pressure between $M_\infty = 1.6$ and $M_\infty = 3.5$. The damping of the first resonant mode was about 25% higher for separated flow than for attached flow, but otherwise the damping of all modes was about the same for either flow condition.

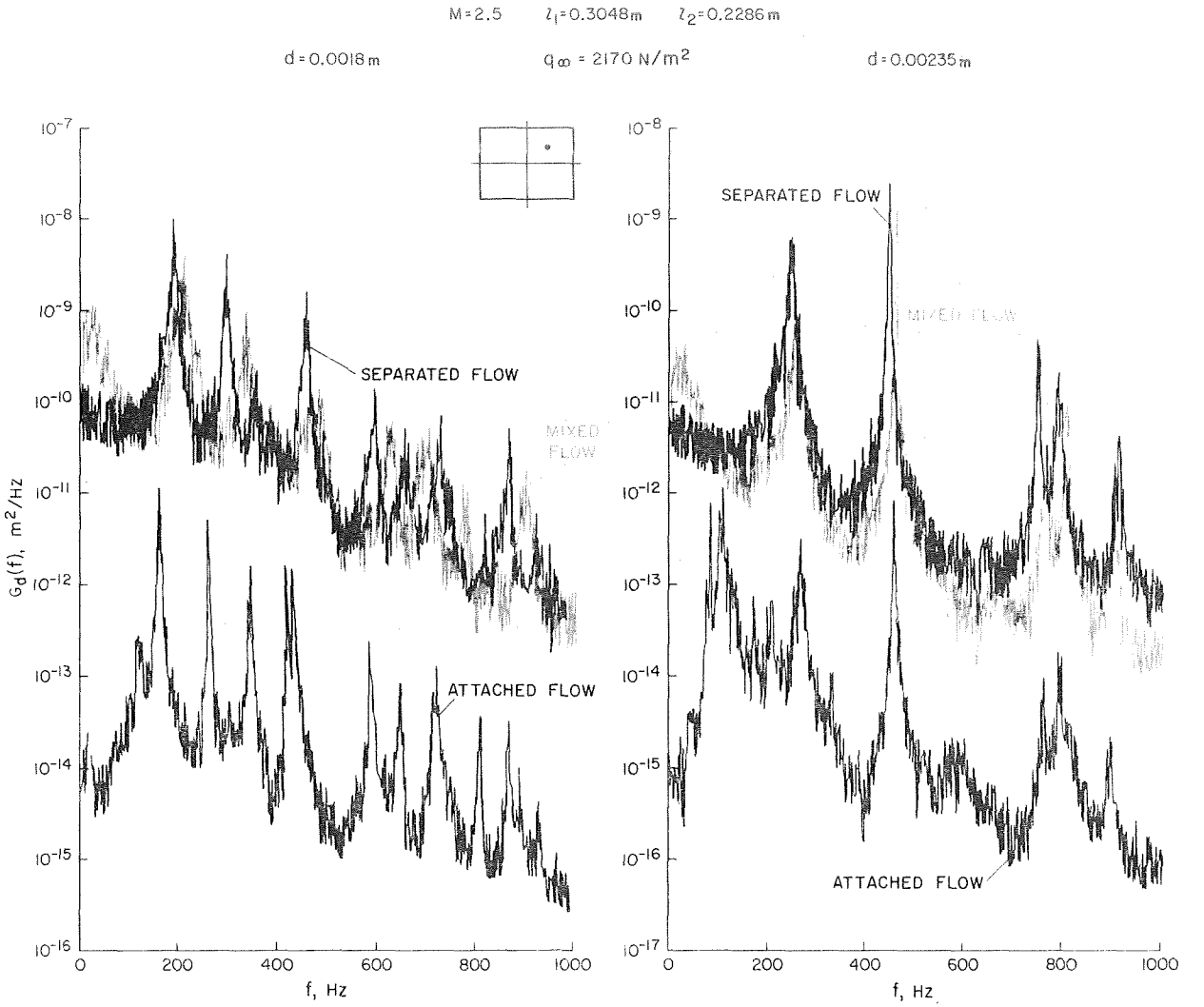

Figure 22. Comparison of panel response due to excitations of attached and separated boundary layer and oscillating shock waves.

5. REFERENCES

1. Corcos, G. M. and Liepmann, H. W.: On the Contribution of Turbulent Boundary Layers to the Noise Inside a Fuselage, NACA TM 1420, 1956.

2. Ribner, H. S.: Boundary-Layer-Induced Noise in the Interior of Aircraft, University of Toronto, U. T. I. A. Report 37, 1956.

3. Kraichnan, R. H.: Noise Transmission from Boundary Layer Pressure Fluctuations, J. Acoust. Soc. Am. 1 Jan. 1957.

4. Chyu, W. J. and Hanly R. D.: Power- and Cross-Spectra and Space-Time Correlations of Surface Fluctuating Pressures at Mach Numbers Between 1.6 and 2.5, NASA TN D-5440.

5. Speaker, W. F. and Ailman, C. M.: Spectra and Space-Time Correlations of the Fluctuating Pressures at a Wall Beneath a Supersonic Turbulent Boundary Layer Perturbed by Steps and Shock Waves. Douglas Rep., SM-49806, Nov. 1965.

6. Lowson, M. V.: Prediction of the Inflight Fluctuating Pressures on Space Vehicles, Wyle Laboratories Report, WR 65-26, Dec. 1965.

7. Coe, C. F.: Surface-Pressure Fluctuations Associated with Aerodynamic Noise, NASA SP-207, pp. 409-424, 1969.

8. Strawderman, W. A.: Turbulent-Induced Plate Vibrations: An Evaluation of Finite and Infinite-Place Models, J. Acoust. Soc. Am., Vol. 45, No. 5, Part 2, 1969.

9. Bozich, D. J.: Spatial Correlation in Acoustic-Structural Coupling, J. Acoust. Soc. Am., 36, 1 Jan. 1964.

10. Wilby, J. F.: The Response of Simple Panels to Turbulent Boundary Layer Excitation, AFFDL-TR-67-70, Oct. 1967.

11. Bull, M. K.: Wall-Pressure Fluctuations Associated with Subsonic Turbulent Boundary-Layer Flow, J. Fluid Mech., Vol. 28, PT. 4, pp. 719, 1967.

12. Chyu, W. J. and Au-Yang, M. K.: Random Response of Rectangular Panels to the Pressure Field Beneath a Turbulent Boundary Layer in Subsonic Flows. NASA TN D-6970, 1972.

13. Willmarth, W. S. and Roos, F. W.: Resolution and Structure of the Wall Pressure Field Beneath a Turbulent Boundary Layer. J. of Fluid Mech., Vol. 22, Part I, pp. 81-94, 1965.

14. Belcher, P. M.: Predictions of Boundary-Layer Turbulence Spectra and Correlations for Supersonic Flight, 5e Congres International D'Acoustique, Liege, Sept. 1965.

15. Chapman, D. R.; Kuehn, D. M.; and Larson, H. K.: Investigation of Separated Flows in Supersonic and Subsonic Streams With Emphasis on the Effect of Transition. NACA TR-1356, 1958.

16. Ffowcs-Williams, J. W.: The Mach Wave Field Radiated by Supersonic Shear Flows, Journal of Fluid Mechanics, Vol. 21, No. 4, pp. 641-657, 1964.

17. Dowell, E. H.: Theoretical Panel Vibration and Flutter Studies Relevant to Space Shuttle, AIAA Paper No. 72-350, AIAA/ASME/SAE 13th Structures, Structural Dynamics, and Materials Conference, 1972.

18. Muhlstein, Lado: Experimental Evaluation of the Aerodynamic Damping of Skin Panels at Low Supersonic Mach Numbers. AIAA Paper No. 72-402. AIAA/ASME/SAE 13th Structures, Structural Dynamics, and Materials Conference, 1972.